Theoretical investigation of the excitonic semiconductor response for varying material thickness: Transition from quantum well to bulk

S. Bischoff
Department of Physics and Material Sciences Center, Philipps-Universität Renthof 5, D-35032 Marburg, Germany and Department of Mathematical Modelling, Technical University of Denmark DK-2800 Lyngby, Denmark

A. Knorr and S. W. Koch
Department of Physics and Material Sciences Center, Philipps-Universität Renthof 5, D-35032 Marburg, Germany
(Received 25 September 1996)

For semiconductor slabs with thicknesses varying from the two-dimensional to the three-dimensional limit the linear optical response is calculated numerically by solving the semiconductor Maxwell-Bloch equations. For short-pulse excitation the spatiotemporal dynamics of the electronic mode structure and the development of exciton-free boundary layers are discussed.
[S0163-1829(97)00112-4]

I. INTRODUCTION

The optical properties of semiconductor materials have been investigated in great detail over the last few years.[1] Within theses studies it has been shown that the linear optical response function (susceptibility) is dominated by bound electron-hole states (excitons) and the Coulomb enhanced scattering states. However, for the description of an optical experiment, not only Coulomb but also light propagation effects play an important role for the calculation of measured spectra, because incident and transmitted field are related by the wave equation. So far, Coulomb and propagation effects are treated self-consistently only for half-space samples (three-dimensional samples, 3D)[2] and for idealized multiple quantum wells (two-dimensional samples, 2D).[3] For the 3D case the famous half-space problem has been solved by Stahl and co-workers[2] using the coherent wave approach. This approach clarified the origin of the exciton-free surface layer (dead layer) and the role of the electronic boundary conditions. On the other hand, the theoretical work in the 2D case has mainly been done for the case where the lowest quantum-confined subband is sufficient to describe the electronic properties. This limits the validity of the 2D theory to structures where the quantum-well width is well below the 3D exciton bohr diameter.

The exciton binding energy and oscillator strength as function of material thickness has been calculated by variational or perturbation methods. A detailed study of the exciton binding energy and oscillator strength for quantum wells with a width up until 20 nm has been made in Ref. 4. Concerning the transition from 2D to 3D structures, theories with fractional-dimensional space,[5,6] where the fractional dimension of the exciton is a fitting parameter, have been developed. A review of the recent literature is given in the paper by Zimmermann.[7] However, in these studies no relations were made to the influence of light propagation in a thin slab. Concerning calculations of optical transmission, reflection, or absorption spectra this has been done, to our knowledge, only for the ideal 2D or 3D case, the transition from the 2D to the 3D regime, especially nonstationary effects such as short-pulse excitation have not been fully investigated. Furthermore, most of the papers in this field are focused on excitons, and less on continuum states. However, due to the redistribution of oscillator strength in linear optics the interplay between exciton and continuum states should be important in the 2D to 3D transition, because the 3D continuum develops from higher 2D subbands.

In this paper, we present theoretical calculations of transmission spectra for semiconductor slabs with different thicknesses by solving the semiconductor Bloch equations (SBE) in combination with Maxwell's equations. As a reference we use the ideal 2D case with one quantized state (subband). The transition to the 3D case is then investigated by including more and more quantized states with increasing material width. Similar to the coherent wave approach, the boundary conditions are determined by the electronic wave functions. This method enables us to calculate the transmission spectrum for a finite material width without additional boundary conditions. Numerical calculations are presented for samples smaller than the wavelength of light. For the case of optical excitation with short laser pulses we show how the so called exciton dead layer, which is known from a stationary analysis in the half-space geometry, develops as a function of time.

II. OBSERVABLES

The quantities of interest in an optical experiment are the spectral transmission, α, or the reflection coefficient R:

$$\alpha(\omega) = -\ln\left(\frac{I_t(\omega)}{I_0(\omega)}\right), \tag{1}$$

$$R(\omega) = \left(\frac{I_r(\omega)}{I_0(\omega)}\right), \tag{2}$$

where I_t, I_r, I_0 are the transmitted, reflected, and incident intensity of the transversal field E_T. From such measurements, the absorbed irradiance ω, i.e., the amount of light per unit length that stays in the sample, can be calculated from

$$w(\omega)=\left[1-\left(\frac{I_t(\omega)}{I_0(\omega)}\right)-\left(\frac{I_r(\omega)}{I_0(\omega)}\right)\right]. \tag{3}$$

In the following we focus mainly on the transmission, which is directly measurable.

III. BASIC EQUATIONS

To compute the observable quantities, the wave equation has to be solved to determine the transverse electric field E_T:

$$\left(\nabla^2-\frac{1}{c^2}\frac{\partial^2}{\partial t^2}\right)E_T=\frac{4\pi}{c_0^2}\frac{\partial j}{\partial t}, \tag{4}$$

where we implicitely assume that the total current j is purely transverse. This is always fulfilled for the plane wave excitation considered throughout this paper. c is the speed of light in the semiconductor and c_0 is the speed of light in vacuum. As is well known, the current j or the polarization P is the source term for the electric field.[1] Thus, to obtain the measurable quantities, the equation of motion for the polarization is needed. The polarization is obtained from

$$j=\frac{\partial P}{\partial t}=\left\langle \psi^\dagger\frac{\hbar e}{i2m_0}\nabla_{\mathbf{r}}\psi\right\rangle+\text{H.a.}, \tag{5}$$

where $\Psi^\dagger$ and Ψ are the Heisenberg creation and annihilation operators, respectively. m_0 is the bare electron mass, $\hbar$ is Planck's constant, and e is the electronic charge.

As usual, the equations of motion for the Heisenberg creation and annihilation operators are determined by the total Hamiltonian which, besides the free parts, contains the Coulomb interaction of the carriers and the carrier interaction with the light field:

$$H_{\text{el}}=H_{o,\text{el}}+H_{\text{el},l}+H_I, \tag{6}$$

$$H_{0,\text{el}}=\int d^3x\,\psi^\dagger(\vec{r})\left(-\frac{\hbar^2}{2m_0}\Delta+V_L(\vec{r})+V_c(\vec{r})\right)\psi(r), \tag{7}$$

$$H_{\text{el},l}=\int d^3r\,\psi^\dagger(\vec{r})\left(-\frac{\hbar e}{im_0c_0}\vec{A}(\vec{r},t)\vec{\nabla}\right)\psi(\vec{r}), \tag{8}$$

$$H_I=\frac{1}{2}\int d^3r\,d^3r'\,\psi^\dagger(\vec{r})\psi^\dagger(\vec{r}')V(\vec{r}-\vec{r}')\psi(\vec{r}')\psi(\vec{r}). \tag{9}$$

Here $H_{o,\text{el}}$ is free carrier Hamiltonian, which contains the kinetic energy, the lattice potential, and the confinement potential including the boundary conditions at the interfaces between the sample and the outside world. $H_{\text{el},l}$ is the carrier-light interaction Hamiltonian and H_I is the Hamiltonian of the carrier-carrier Coulomb interaction. $\vec{A}(\vec{r},t)$ is the transversal vector potential and $\vec{r}$ is the three-dimensional space coordinate, $\vec{r}=(x,y,z)=(\vec{\rho},z)$. The Coulomb potential, $V(\vec{r})$ is in CGS units,

$$V(\vec{r}')=\frac{e^2}{\varepsilon_0|\vec{r}'|}, \tag{10}$$

where ε_0 is the screening of the Coulomb potential due to off-resonant transitions. To study the basic effects of the 2D to 3D transition we only consider the ideal condition, where the potential V_C which confines the electrons in one direction of the sample is infinite,

$$V_c(z)=\begin{cases}0 \text{ when } |z|<\dfrac{L_z}{2}\\ \infty \text{ when } |z|>\dfrac{L_z}{2},\end{cases} \tag{11}$$

where L_z is the total width of the sample. Effects of a finite confinement potential on the optical susceptibility are discussed, e.g., in Ref. 4.

The tranverse electrical field E_T is determined by the vector potential $\vec{A}(\vec{r})$,

$$\vec{E}_T=-\frac{1}{c_0}\frac{\partial\vec{A}(\vec{r},\vec{t})}{\partial t}\approx\frac{i\omega_L}{c_0}\vec{A}(\vec{r},t), \tag{12}$$

where in the following the slowly varying envelope and rotating wave approximation is applied.

To obtain the polarization, which is the source term in the wave equation, the Heisenberg creation and annihilation operators are expanded in terms of the eigenfunctions of the free particle Hamiltonian because it is more conventient in our approach to solve the equations of motion in momentum space:

$$\psi^\dagger(\vec{r})=\sum_{\vec{k},n,\lambda}a^\dagger_{\vec{k},n,\lambda}\frac{e^{-i\vec{k}\cdot\vec{\rho}}}{L}f^*_{n,\lambda}(z)u^*_\lambda(\vec{k},\vec{r}), \tag{13}$$

$$\psi(\vec{r})=\sum_{\vec{k},n,\lambda}a_{\vec{k},n,\lambda}\frac{e^{i\vec{k}\cdot\vec{\rho}}}{L}f_{n,\lambda}(z)u_\lambda(\vec{k},\vec{r}). \tag{14}$$

Here, $\lambda=c,v$ denotes either the conduction or valence band, respectively. $\vec{k}$ is the in-plane momentum, u_λ is the Bloch function, and L^2L_z represents the volume of the crystal with L^2 being the area of the well. The quantum number of the subband is labeled by the index n. $a_{\vec{k},n,\lambda}$ is the electron annihilation operator and $a^\dagger_{\vec{k},n,\lambda}$ is the electron creation operator of a Bloch electron with the quantum numbers $\vec{k}$, n, λ, respectively. The z dependence of the wave function $f^*_{n,\lambda}(z)$ is for the quantum numbers $n=1, 3, 5, 7, \ldots,$

$$f_{n,\lambda}(z)=\begin{cases}\sqrt{\dfrac{2}{L_z}}\cos\left(n\dfrac{\pi}{L_z}z\right) \text{ when } |z|\leqslant\dfrac{L_z}{2}\\ 0 \text{ when } |z|\geqslant\dfrac{L_z}{2},\end{cases} \tag{15}$$

and for $n=2, 4, 6, 8, \ldots$

$$f_{n,\lambda}(z)=\begin{cases}\sqrt{\dfrac{2}{L_z}}\sin\left(n\dfrac{\pi}{L_z}z\right) \text{ when } |z|\leqslant\dfrac{L_z}{2}\\ 0 \text{ when } |z|\geqslant\dfrac{L_z}{2}.\end{cases} \tag{16}$$

The Heisenberg equation of motion for the electron operators yields within linear optical response theory,

$$\frac{\partial p_{\vec{k}}^{n_1^v,n_2^c}}{\partial t} = -i(\omega_{\vec{k}}^{n_1^v,n_2^c} - i\gamma)p_{\vec{k}}^{n_1^v,n_2^c} + \frac{i}{\hbar}d_{cv}E_{\vec{k}}^{n_1^v,n_2^c} + \frac{i}{\hbar}\sum_{\vec{q}\neq\vec{0},q_1^v,q_2^c} p_{\vec{k}-\vec{q}}^{q_1^v,q_2^c} V_{\vec{q}}^{n_2^c,q_1^v,n_1^v,q_2^c}, \tag{17}$$

where $\omega_k^{n_1^v,n_2^c} = \omega_k^{n_2^c} - \omega_k^{n_1^v} - \omega_L$ is the transition renormalized frequency of the quantized states in the slowly varying envelope approximation, γ is a phenomenologically introduced decay rate of the polarization function ($p_{\vec{k}}^{n_1^v,n_2^c} = \langle a_{\vec{k},n_1,v}^{\dagger} a_{\vec{k},n_2,c}\rangle$), and d_{cv} is the dipole moment. n_x^{λ} and q_x^{λ} are quantum numbers of the quantized states and $\vec{q}$ is an in-plane momentum vector. Since we are interested only in the optical spectra we have neglected terms that are attributed to intraband transitions. $V_{\vec{q}}^{n_2^c,q_1^v,n_1^v,q_2^c}$ is the unscreened Coulomb potential, which for $n_x^{\lambda_x} = 1, 3, 5, 7, \ldots$ is given as

$$V_{\vec{q}}^{n_1^{\lambda_1},n_2^{\lambda_2},n_3^{\lambda_3},n_4^{\lambda_4}} = \frac{2\pi e^2}{L^2\epsilon_0 q}\frac{2}{\pi^2}\left(q\frac{L_z}{\pi}\right)^2(e^{-qL_z}-1)\left[\frac{\cos\left((n_2^{\lambda_2}-n_3^{\lambda_3})\frac{\pi}{2}\right)}{\left(q\frac{L_z}{\pi}\right)^2+(n_2^{\lambda_2}-n_3^{\lambda_3})^2}+\frac{\cos\left((n_2^{\lambda_2}+n_3^{\lambda_3})\frac{\pi}{2}\right)}{\left(q\frac{L_z}{\pi}\right)^2+(n_2^{\lambda_2}+n_3^{\lambda_3})^2}\right]$$

$$\times\left[\frac{\cos\left((n_1^{\lambda_1}-n_4^{\lambda_4})\frac{\pi}{2}\right)}{\left(q\frac{L_z}{\pi}\right)^2+(n_1^{\lambda_1}-n_4^{\lambda_4})^2}+\frac{\cos\left((n_1^{\lambda_1}+n_4^{\lambda_4})\frac{\pi}{2}\right)}{\left(q\frac{L_z}{\pi}\right)^2+(n_1^{\lambda_1}+n_4^{\lambda_4})^2}\right]+\frac{2\pi e^2}{L^2\epsilon_0 q}\frac{1}{\pi}q\frac{L_z}{\pi}\frac{1}{\left(q\frac{L_z}{\pi}\right)^2+(n_2^{\lambda_2}-n_3^{\lambda_3})^2}$$

$$\times[\delta_{n_1^{\lambda_1}-n_4^{\lambda_4},n_2^{\lambda_2}-n_3^{\lambda_3}}(1+\delta_{n_1^{\lambda_1}-n_4^{\lambda_4},0})+\delta_{n_1^{\lambda_1}+n_4^{\lambda_4},n_2^{\lambda_2}-n_3^{\lambda_3}}]+\frac{2\pi e^2}{L^2\epsilon_0 q}\frac{1}{\pi}q\frac{L_z}{\pi}\frac{1}{\left(q\frac{L_z}{\pi}\right)^2+(n_2^{\lambda_2}+n_3^{\lambda_3})^2}$$

$$\times(\delta_{n_1^{\lambda_1}-n_4^{\lambda_4},n_2^{\lambda_2}+n_3^{\lambda_3}}+\delta_{n_1^{\lambda_1}+n_4^{\lambda_4},n_2^{\lambda_2}+n_3^{\lambda_3}}),\quad \text{where } q=|\vec{q}|. \tag{18}$$

The expression for the Coulomb potential for other combinations of quantum numbers is similar to the one given in Eq. (18). A full listing of the Coulomb potential is given in Appendix A.

The coupling to the light field is treated semiclassically and enters through $E_{\vec{k}}^{n_1^v,n_2^c}$,

$$E_{\vec{k}}^{n_1^v,n_2^c} = \int_{-L_z/2}^{L_z/2} dz\, f_{n_1^v}^{*}(z)E_T(z)f_{n_2^c}(z), \tag{19}$$

where $E_T(z)$ is determined by solving the wave equation. Often, in the description of optical experiments with semiconductors it is assumed that optical absorption occurs between quantized states with an equal quantum number $n_1 = n_2$. This approximation assumes that the electric field is not or weakly space dependent. However, as we see from the expression for $E_{\vec{k}}^{n_1^v,n_2^c}$ transitions between states with unequal quantum number are allowed for spatially varying fields. In general, one can only neglect the transitions between quantized states with unequal quantum number, as long as the material width (L_z) is much shorter than the wavelength of the exciting pulse. This case yields $E_{\vec{k}}^{n_1^v,n_2^c} \sim \delta_{n_1^v,n_2^c}$.

Assuming the incoming light field to consist of plane waves, we can solve Maxwell's equation in the frequency domain analytically. Again we only give the solution for the quantum numbers $n_x^{\lambda^x} = 1, 3, 5, 7, \ldots$ (a full listing of the solution is given in Appendix B),

$$E_T^{n_1^v,n_2^c}(z,\omega) = \frac{4\pi}{L_z}\frac{c^2}{c_0^2}d_{cv}P_{n_1^v,n_2^c}(\omega)\cdot\left(\frac{\cos\left((n_1^v-n_2^c)\frac{\pi}{L_z}z\right)}{(n_1^v-n_2^c)^2\frac{\pi^2c^2}{L_z^2\omega^2}-1}+\frac{\cos\left((n_1^v+n_2^c)\frac{\pi}{L_z}z\right)}{(n_1^v+n_2^c)^2\frac{\pi^2c^2}{L_z^2\omega^2}-1}\right)$$

$$+t_{n_1^v,n_2^c}(\omega)e^{i(\omega/c)z}+r_{n_1^v,n_2^c}(\omega)e^{-i(\omega/c)z}. \tag{20}$$

Here, $t_{n_1^v,n_2^c}$ and $r_{n_1^v,n_2^c}$ are functions, which have to be determined by applying the boundary conditions for the electrical field at the interfaces (continuity of field and first derivative). The polarization $P_{n_1^v,n_2^c}$ is defined as

$$P_{n_1^v,n_2^c}=\frac{1}{L^2}\sum_{\vec{k}} p_{\vec{k}}^{n_1^v,n_2^c}. \tag{21}$$

Using the boundary conditions, the electric field can be determined to be (index matched structure)

$$\begin{aligned}
E_T(z,\omega)=E_{\rm in}e^{ik_z z}-2\pi\frac{\omega}{c}\frac{c^2}{c_0^2}d_{cv}\frac{e^{ik_z(L_z/2)}}{k_z\frac{L_z}{2}}\frac{e^{ik_z z}+e^{-ik_z z}}{2}\sum_{n_1^v,n_2^c}P_{n_1^v,n_2^c}(\omega)\left(\frac{\cos\left((n_1^v-n_2^c)\frac{\pi}{2}\right)}{(n_1^v-n_2^c)^2\frac{\pi^2c^2}{L_z^2\omega^2}-1}+\frac{\cos\left((n_1^v+n_2^c)\frac{\pi}{2}\right)}{(n_1^v+n_2^c)^2\frac{\pi^2c^2}{L_z^2\omega^2}-1}\right)\\
+2\pi\frac{\omega}{c}\frac{c^2}{c_0^2}d_{cv}\frac{1}{k_z\frac{L_z}{2}}\sum_{n_1^v,n_2^c}P_{n_1^v,n_2^c}(\omega)\left(\frac{\cos\left((n_1^v-n_2^c)\frac{\pi}{L_z}z\right)}{(n_1^v-n_2^c)^2\frac{\pi^2c^2}{L_z^2\omega^2}-1}+\frac{\cos\left((n_1^v+n_2^c)\frac{\pi}{L_z}z\right)}{(n_1^v+n_2^c)^2\frac{\pi^2c^2}{L_z^2\omega^2}-1}\right)\\
-2\pi\frac{\omega}{c}\frac{c^2}{c_0^2}d_{cv}\frac{e^{ik_z(L_z/2)}}{k_z\frac{L_z}{2}}\frac{e^{ik_z z}+e^{-ik_z z}}{2}\sum_{m_1^v,m_2^c}P_{m_1^v,m_2^c}(\omega)\left(\frac{\cos\left((m_1^v-m_2^c)\frac{\pi}{2}\right)}{(m_1^v-m_2^c)^2\frac{\pi^2c^2}{L_z^2\omega^2}-1}-\frac{\cos\left((m_1^v+m_2^c)\frac{\pi}{2}\right)}{(m_1^v+m_2^c)^2\frac{\pi^2c^2}{L_z^2\omega^2}-1}\right)\\
+2\pi\frac{\omega}{c}\frac{c^2}{c_0^2}d_{cv}\frac{1}{k_z\frac{L_z}{2}}\sum_{m_1^v,m_2^c}P_{m_1^v,m_2^c}(\omega)\left(\frac{\cos\left((m_1^v-m_2^c)\frac{\pi}{L_z}z\right)}{(m_1^v-m_2^c)^2\frac{\pi^2c^2}{L_z^2\omega^2}-1}-\frac{\cos\left((m_1^v+m_2^c)\frac{\pi}{L_z}z\right)}{(m_1^v+m_2^c)^2\frac{\pi^2c^2}{L_z^2\omega^2}-1}\right)\\
+2\pi\frac{\omega}{c}\frac{c^2}{c_0^2}d_{cv}\frac{e^{ik_z(L_z/2)}}{k_z\frac{L_z}{2}}\frac{e^{ik_z z}+e^{-ik_z z}}{2}\sum_{m_1^v,n_2^c}P_{m_1^v,n_2^c}(\omega)\left(\frac{\sin\left((m_1^v-n_2^c)\frac{\pi}{2}\right)}{(m_1^v-n_2^c)^2\frac{\pi^2c^2}{L_z^2\omega^2}-1}+\frac{\sin\left((m_1^v+n_2^c)\frac{\pi}{2}\right)}{(m_1^v+n_2^c)^2\frac{\pi^2c^2}{L_z^2\omega^2}-1}\right)\\
+2\pi\frac{\omega}{c}\frac{c^2}{c_0^2}d_{cv}\frac{1}{k_z\frac{L_z}{2}}\sum_{m_1^v,n_2^c}P_{m_1^c,n_2^v}(\omega)\left(\frac{\sin\left((m_1^v-n_2^c)\frac{\pi}{L_z}z\right)}{(m_1^v-n_2^c)^2\frac{\pi^2c^2}{L_z^2\omega^2}-1}+\frac{\sin\left((m_1^v+n_2^c)\frac{\pi}{L_z}z\right)}{(m_1^v+n_2^c)^2\frac{\pi^2c^2}{L_z^2\omega^2}-1}\right)\\
+2\pi\frac{\omega}{c}\frac{c^2}{c_0^2}d_{cv}\frac{e^{ik_z(L_z/2)}}{k_z\frac{L_z}{2}}\frac{e^{ik_z z}+e^{-ik_z z}}{2}\sum_{n_1^v,m_2^c}P_{n_1^v,m_2^c}(\omega)\left(\frac{\sin\left((m_2^c-n_1^v)\frac{\pi}{2}\right)}{(m_2^c-n_1^v)^2\frac{\pi^2c^2}{L_z^2\omega^2}-1}+\frac{\sin\left((n_1^v+m_2^c)\frac{\pi}{2}\right)}{(n_1^v+m_2^c)^2\frac{\pi^2c^2}{L_z^2\omega^2}-1}\right)\\
+2\pi\frac{\omega}{c}\frac{c^2}{c_0^2}d_{cv}\frac{1}{k_z\frac{L_z}{2}}\sum_{n_1^v,m_2^c}P_{n_1^v,m_2^c}(\omega)\left(\frac{\sin\left((m_2^c-n_1^v)\frac{\pi}{L_z}z\right)}{(m_2^c-n_1^v)^2\frac{\pi^2c^2}{L_z^2\omega^2}-1}+\frac{\sin\left((n_1^v+m_2^c)\frac{\pi}{L_z}z\right)}{(n_1^v+m_2^c)^2\frac{\pi^2c^2}{L_z^2\omega^2}-1}\right).
\end{aligned} \tag{22}$$

Here, n_x^λ labels the quantized states 1, 3, 5, ... and m_x^λ labels the quantized states 2, 4, 6, ... ω is the optical carrier frequency, and $k_z=\omega/c$. $E_{\rm in}$ is the electrical field of the incoming light field.

The term $E_{\vec{k}}^{n_1^v,n_2^c}$ is now calculated by inserting Eq. (22) into Eq. (19). Equation (17) can be solved to yield the polarizations of the different transitions which in turn determine the transversal energy field and thus the transmission. In this way, linear spectra can be calculated in the frequency domain. Our approach uses a time domain integration. The transformation of the energy field to the time domain is done by assuming the spectral frequency to be equal to the optical carrier frequency ω_L, which is an approximation similar to the slowly varying envelope approximation. This approximation allows us to calculate short-pulse excitation and nonstationary effects very efficiently. Note however that this approximation breaks down at $(n_1^v\pm n_2^c)(\pi^2c^2/L_z^2\omega_L^2)-1=0$.

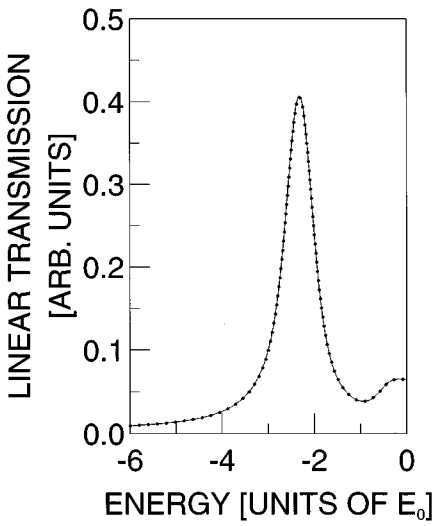

FIG. 1. The linear transmission spectrum for $L_z = 10$ nm, where the off-diagonal transisions are included (—) and when the off-diagonal transisions are neglected $(\cdots)$. Two subbands must be included in the calculations. E_0 is the ideal 3D exciton binding energy.

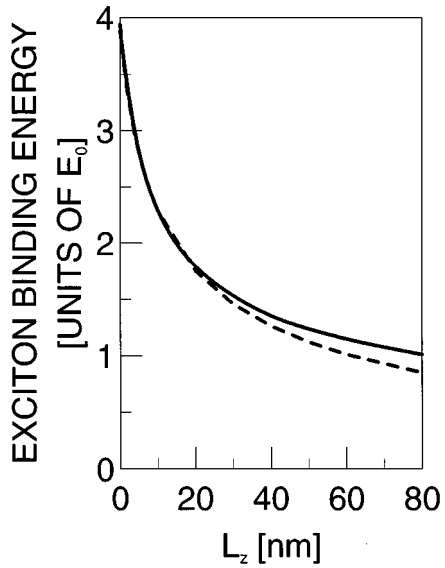

FIG. 2. The binding energy of the 1s exciton for GaAs as a function of the material thickness L_z, (—). (- - -) 1s exciton binding energy, when only one quantized state is considered. E_0 is the ideal 3D exciton binding energy.

In this case the sample thickness is a multiple of $\lambda/2$. So, in the following we will restrict our investigation to the case where $L_z < \lambda/2$. However, we expect to obtain the basic features of the 2D to 3D transition to take place before $L_z \approx \lambda/2$.

IV. STATIONARY TRANSMISSION SPECTRA

In the following stationary transmission spectra for the case of GaAs are presented. The relative electron (m_c/m_0), relative hole mass (m_v/m_0), the refractive index n_g, and the phenomenological dephasing rate γ used in our calculations are given in Table I. m_0 is the free electron mass.

In Fig. 1 a comparison of transmission spectra including and neglecting nondiagonal subband transitions in the interaction matrix Eq. (19) is given. The figure confirms that for a sample width smaller than the wavelength of light the influence of the nondiagonal terms is indeed negligible.

In the following we restrict our analysis to samples smaller than the wavelength of light where the neglection of transitions between states with different subband quantum numbers is an excellent approximation. In Fig. 2 we show the exciton binding energy obtained from the transmission spectrum as a function of the material thickness L_z. For comparison we have included the curve for the exciton binding energy, if only one quantized state is considered. We see that one quantized state is only sufficient to describe the exciton binding energy, as long as the quantum well width is less than 15 nm, which is about 1.25 times the 3D bohr radius. Furthermore, we see that the ideal 2D exciton binding energy only is obtained for a material width of less than 1 nm, while the ideal 3D exciton binding energy is almost reached for $L_z = 80$ nm.

Figure 3 shows the peak height of the lowest subband 1s exciton in the transmission spectrum for three different

TABLE I. Parameter values for GaAs.

Symbol	Unit	Value
m_v	m_0	0.3770
m_c	m_0	0.0655
n_g		3.6786
a_0	Å	128
γ_k	s^{-1}	2×10^{12}
$d_c v$	(e) Å	e 7.2

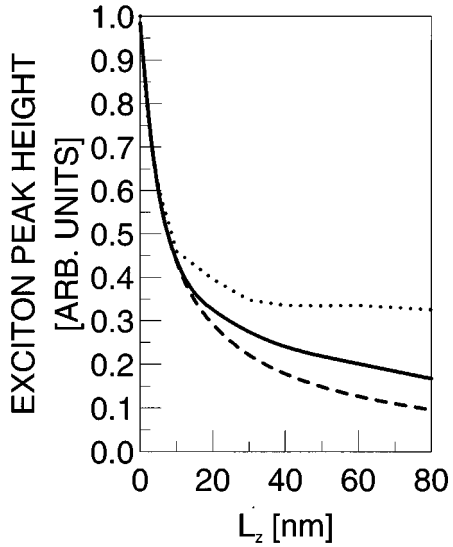

FIG. 3. The 1s exciton peak height in the linear transmission spectrum as a function of the material thickness $(\cdots)$ and the peak height, if only one quantized state is included (- - -). The solid line shows the lowest subband contribution to the peak height, when all quantized states are included.

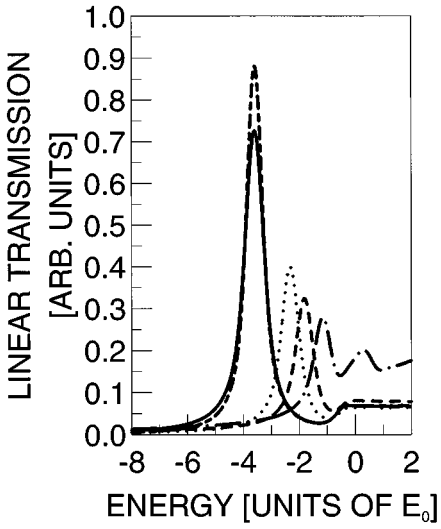

FIG. 4. The linear transmission spectrum for the material thickness of 1 nm (—), 10 nm (. . .), 20 nm (- - -), and 60 nm (- · -). The imaginary part of $\chi(\omega,z=0)$ is plotted for $L_z = 1$ nm (– - –). E_0 is the ideal 3D exciton binding energy.

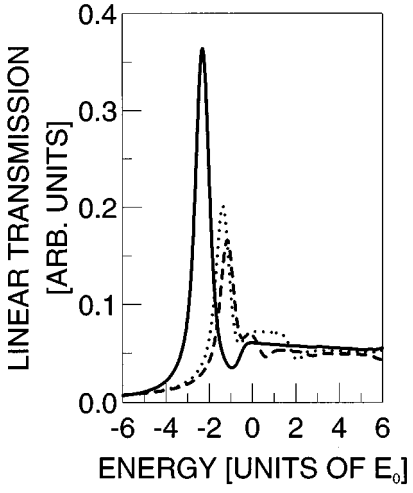

FIG. 5. The linear transmission spectrum for the material thickness of 10 nm (—), 40 nm (. . .), and 60 nm (- · -). The propagation equation and SBE are solved by inclusion of higher subbands. The linear transmission is calculated by only considering the lowest subband. E_0 is the 3D exciton binding energy.

cases. The dotted line is the 1s exciton peak height, when all subband transitions are taken into account. The dashed line represents the case when the transmission spectrum is calculated by considering only the lowest subband. Finally, the solid line is the 1s exciton peak height in the case where the wave-propagation equation and the SBE are solved by including all subband contributions; however, only the contributions of the lowest subband to the linear transmission are plotted. The dashed line in Fig. 3 shows again the importance of including more than one subband for a material width larger than 15 nm. The difference between the solid and the dotted line indicates how the higher subband contributions increase the peak height of the first subband exciton. The change of the transmission spectrum due to the Coulomb potential is elucidated by the solid line. The difference between the solid and dotted line depends to some degree on the chosen phenomenological decay rate, which determines the width of the 1s excitons. The tail of the second and higher subband transitions lines increase the lowest 1s exciton peak height depending on the decay rate and material width. To illustrate this behavior further, the transmission spectra for a few material widths corresponding to the dotted line are shown in Figs. 4 and 6, while a few transmission spectra corresponding to the solid line are plotted in Fig. 5. The linear transmission spectra shown in Fig. 4 are for the material width $L_z = 1$ nm, 10 nm, 20 nm, and 60 nm. We see with increasing material width a significant decrease of both exciton binding energy and peak height.

The decrease in the exciton binding energy and the decrease of the exciton peak height is a result of the dependence of the Coulomb potential on the sample thickness. However, the inclusion of more than one subband leads to an increase in the exciton binding energy and peak height compared to the calculations where only one subband is considered. A numerical analysis shows that this increment of the binding energy and the peak height is caused by the Coulomb matrix elements, which are off diagonal with respect to the subband indices. Thus it can be concluded that with increasing sample width the off-diagonal Coulomb matrix elements cause a gradual transfer of oscillator strength from the energetically higher exciton peaks to the lowest 1s exciton peak, see Fig. 6. This is elucidated by Fig. 5, which shows the ''pure'' lowest subband 1s exciton plus continuum for a different sample thickness. The second and higher 1s exciton plus their continuum are omitted (subtracted) in this figure. There is a significant reduction in the continuum of the transmission spectrum at the positions of the higher subband excitons, which is a result of the transfer of oscillator strength by the Coulomb potential.

In Fig. 4 we have for $L_z = 1$ nm included a plot of the imaginary part of the susceptibility at the center of the sample (short-long dashed line). The difference between the

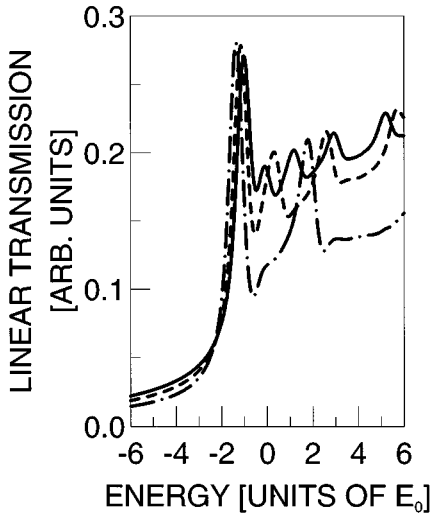

FIG. 6. The linear transmission spectrum for the material thickness of 40 nm (– · –), 60 nm (- - -), and 80 nm (—) E_0 is the ideal 3D exciton binding energy.

susceptibility and the linear transmission spectrum verifies that the inclusion of the propagation effects are important. We see that the inclusion of the propagation effects result in a reduction in the 1*s* exciton peak height and significant broadening of the 1*s* exciton. This corresponds to the radiative damping mechanism for exciton polaritons in low dimensional systems.[3] Furthermore, since the polarization is space dependent the definition of an effective space independent susceptibility is somewhat arbitrary, especially when more than one subband is needed to describe the optical properties of the sample.

In Fig. 6 the 2D to 3D transition is indicated by showing the vanishing oscillator strength of the second and higher subband 1*s* excitons with increasing material thickness. The change in exciton binding energy for the first subband 1*s* exciton is small, when increasing the material width from $L_z = 40$ nm to $L_z = 80$ nm. The peak height is also almost unchanged. However it should be noted that this is due to a compensation effect since the change in peak height also depends on the linewidth of the higher subbands, which can compensate for the peak decrease with increasing thickness. Nevertheless, the second subband exciton and higher subband excitons lose a significant amount of oscillator strength with increasing material thickness. Thus, the 3D absorption spectrum is expected to be obtained for a thickness where the second and higher subband 1*s* excitons will have an oscillator strength comparable to their continuum.

The complexity of the Coulomb potential in our approach makes it computationally very demanding to study the full transition to the 3D absorption spectrum. One should keep in mind that in this paper we have shown that the transitions between unequal quantum numbers are negligible when the material width is much smaller than the wavelength. However, the full transition to the 3D spectrum is expected to occur at a material width comparable with the optical wavelength. In this case the transitions between unequal quantum numbers have to be taken into account and the Fourier transform of the solution of the wave-propagation equation has to be calculated without any approximations. This will increase the computational demands considerably. On the other hand, the studies given above for a thickness smaller than half the wavelength already yield the basic transition mechanisms.

V. NONSTATIONARY EFFECTS

In the prevoius section we studied how the transition from the 2D to 3D transmission spectrum takes place for different sample thicknesses. The spectra contain the information to which extent certain electronic states of the material system are excited after the light is switched off. However, the same information is contained as well in the temporal interference of the polarization of different electronic states. In Fig. 7 we present a logarithmic plot of the incident and transmitted electrical field for the case of a 60 nm sample, where the input pulse is a hyperbolic-secant-shaped pulse with a full width at half maximum (FWHM) of 80 fs. In the figure we have also included a logarithmic plot of the absolute value of the polarization at the center of the sample. The transmitted electrical field and the polarization exhibit a dominant oscillation with a period of 260 fs. This oscillation is due to the beating of the lowest subband 1*s* exciton with the third subband 1*s* exciton (260 fs). The beating between the second and first subband is not seen in the figure since the corresponding period is about 688 fs. However, the beating between the first subband and energetic higher excitons than the second is visible in the figure as a superposition of oscillations with different periods and different oscillator strengths weightened by the pulse spectra.

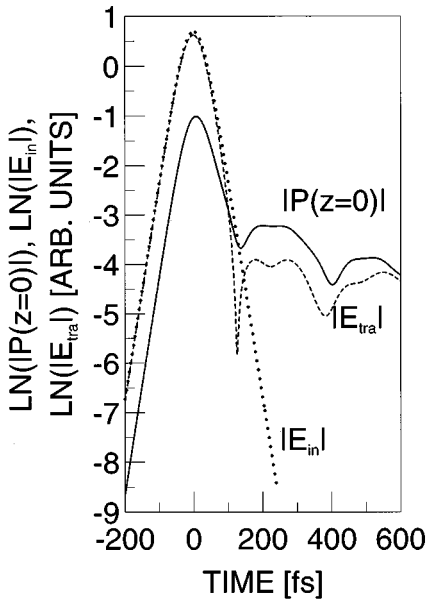

FIG. 7. Plot of the incident, E_{in}, transmitted, E_{tra}, electrical field, and the absolute value of the polarization at the center of the sample. The material thickness is $L_z = 60$ nm.

Figure 8 shows the dynamic evolution of the polarizations

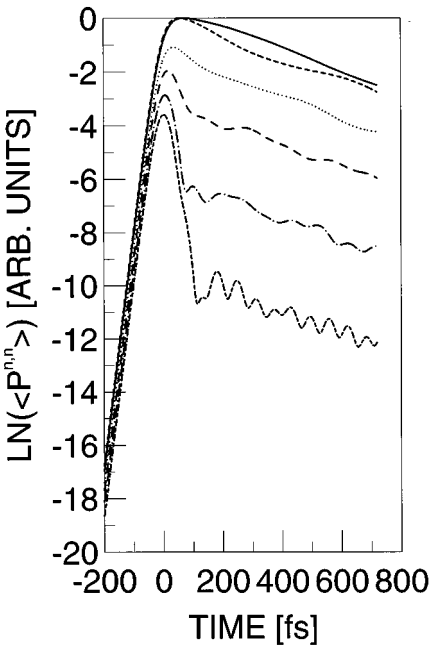

FIG. 8. The polarization ($\langle P^{n,n}\rangle = (1/L^2)\Sigma_k |p_k^{n,n}|^2$) as function of time after excitation by a pulse with FWHM of 80 fs. The material thickness is $L_z = 60$ nm. The different curves are for the subband polarizations $\langle P^{1,1}\rangle$ (—), $\langle P^{2,2}\rangle$ (- - -), $\langle P^{3,3}\rangle$ ($\cdots$), $\langle P^{4,4}\rangle$ (– –), $\langle P^{5,5}\rangle$ (– · –), and $\langle P^{6,6}\rangle$ (– - –).

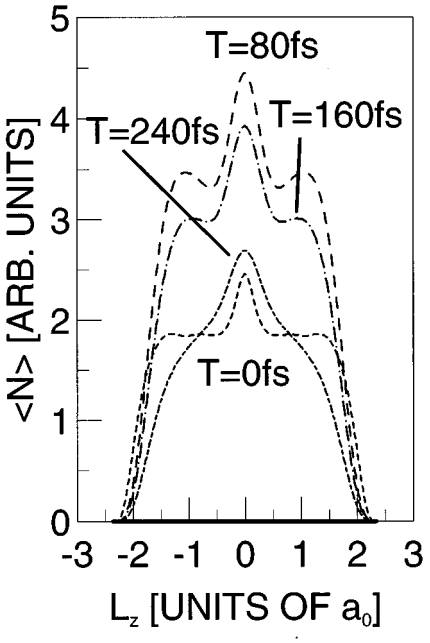

FIG. 9. The electron density ($\langle N\rangle=(1/L^2)\Sigma_{k,n}|p_k^{n,n}|^2$) as function of the space coordiante z after excitation by a pulse with a FWHM of 80 fs. The material thickness is $L_z = 60$ nm. The polarization is shown for the times -200 fs (—), -80 fs ($\cdots$), 0 fs (- - -), 80 fs (– –), 160 fs (– · –), and 240 fs (– - –). a_0 is the ideal 3D bohr radius.

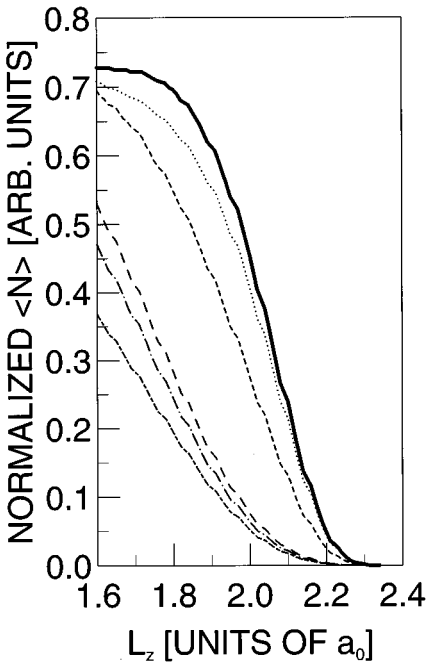

FIG. 10. The normalized electron density $[\langle N\rangle=(1/L^2)\Sigma_{k,n}|p_k^{n,n}|^2]$ as function of the space coordiante z after excitation by a pulse with FWHM of 80 fs. All curves have been normalized to a height of one. The material thickness is $L_z = 60$ nm. The polarization is shown for the times -200 fs (—), -80 fs ($\cdots$), 0 fs (- - -), 80 fs (– –), 160 fs (– · –), and 240 fs (– - –). a_0 is the ideal 3D bohr radius.

of different subbands. It can be recognized that after the pulse is switched on all states develop according to their respective oscillator strength and decay after the pulse maximum, corresponding to their detuning with respect to the pulse. Thus, at different times different subbands contribute to the development of the total electron density, because the subband polarizations determine the weight of the z-dependent confinement functions. The expectation value of the electron density is given by

$$\langle N\rangle=\frac{1}{L^2}\sum_{k,n_1}|P_k^{n_1,n_1}|^2. \tag{23}$$

It should be noted that Eq. (23) only is valid when the transitions between states with unequal quantum number can be neglected.

Figure 9 shows the resulting electron density as a function of the space coordinate z at the time $T=-200$ fs, -80 fs, 0 fs, 80 fs, 160 fs and 240 fs. The time is measured with respect to the pulse peak. The excitation pulse is again chosen to be a hyperbolic-secant pulse with a FWHM of 80 fs and the material thickness is 60 nm. Note that the space axis has been normalized with respect to the 3D exciton Bohr radius. The figure shows the development of an electronic mode structure, which is determined by the length of the material, similar to the optical mode structure in a laser cavity. We see an almost homogenous electron density in the structure with a characteristic peak at the sample center before the pulse peak has passed through the sample. The peak at the center of the sample is a result of the early development of an electron mode structure. Not all transitions are equally excited, as seen in Fig 8. The peak at the center in Fig. 9 corresponds to the highest odd ($n_x^\lambda = 1, 3, 5, \ldots$) quantized state, which contributes significantly to the electron-hole density expectation value. The observation of an almost homogenous electron density agrees well with the common approximation that the absorption spectrum is space independent in a semiconductor structure. However, on the trailing edge of the optical pulse the picture changes. The almost spatially homogenous electron density at early times and the developement of the electronic mode structure can be understood when we look at the expectation value of the polarization for the different subband transitions, Fig. 8. The resulting polarization adiabatically follows the optical pulse more and more. This explains the almost homogenous polarization at early times. The material ''does not know'' the spectral width of the exciting pulse, and so all states (frequencies) are excited by the pulse front. However, with time the spectral properties of the exciting pulse become noticeable and the electronic mode structure develops.

The solution of the half-space problem[2] shows that the stationary electronic mode-structure exhibits a characteristic exciton free layer of the order of one bohr radius at the interface, the so called dead layer. Figure 10 shows the space dependent electron density near the material interface for different times corresponding to the graphs in Fig. 9. However, the curves in Fig. 10 have been normalized to a peak height of one. The development of an exciton-free layer (dead layer) with time can be observed near the material interface. The width of the dead layer is for $L_z = 60$ nm only one-third of the 3D bohr radius, while the exciton-free layer (dead layer) in the half-space problem has a width of approxi-

mately one bohr radius.[2] This shows that our results have still not reached the ideal 3D case.

VI. SUMMARY

In summary we have derived the equations for the optical properties of an arbitrary thick semiconductor sample, including Coulomb and light propagation effects. For sample thicknesses less than half the wavelength we have described the basic effects of how the transition from the 2D to 3D regime of semiconductor material takes place. The change of the 2D transmission spectrum towards the 3D transmission spectrum is explained by showing the importance of the off-diagonal Coulomb potential elements, which increase the exciton binding energy and transfers oscillator strength from higher $1s$ excitons to the lowest quantized state $1s$ exciton. Furthermore, we see the development of a dead layer with material thickness, which is an important factor in the theories applied for solving the half-space problem.

ACKNOWLEDGMENTS

This work has been supported by the Deutsche Forschungsgmeinschaft. S. B. acknowledges the support by the Comission of the European Communities.

APPENDIX A: THE COULOMB POTENTIAL MATRIX ELEMENTS

In this appendix we have written down the expressions for the Coulomb potential for the different combinations of quantum numbers. Here, $n_x^{\lambda_x}$ label the quantized states $n_x^{\lambda_x} = 1, 3, 4, 7, \ldots$, and $m_x^{\lambda_x}$ label the quantized states $m_x^{\lambda_x} = 2, 4, 6, 8, \ldots$.

$$
\begin{aligned}
V_{\vec{q}}^{n_1^{\lambda_1},n_2^{\lambda_2},n_3^{\lambda_3},n_4^{\lambda_4}} = {} & \frac{2\pi e^2}{L^2\epsilon_0 q}\,\frac{2}{\pi^2}\left(q\frac{L_z}{\pi}\right)^2(e^{-qL_z}-1)\left[\frac{\cos\left((n_2^{\lambda_2}-n_3^{\lambda_3})\frac{\pi}{2}\right)}{\left(q\frac{L_z}{\pi}\right)^2+(n_2^{\lambda_2}-n_3^{\lambda_3})^2}+\frac{\cos\left((n_2^{\lambda_2}+n_3^{\lambda_3})\frac{\pi}{2}\right)}{\left(q\frac{L_z}{\pi}\right)^2+(n_2^{\lambda_2}+n_3^{\lambda_3})^2}\right]\left[\frac{\cos\left((n_1^{\lambda_1}-n_4^{\lambda_4})\frac{\pi}{2}\right)}{\left(q\frac{L_z}{\pi}\right)^2+(n_1^{\lambda_1}-n_4^{\lambda_4})^2}\right. \\
& \left.+\frac{\cos\left((n_1^{\lambda_1}+n_4^{\lambda_4})\frac{\pi}{2}\right)}{\left(q\frac{L_z}{\pi}\right)^2+(n_1^{\lambda_1}+n_4^{\lambda_4})^2}\right]+\frac{2\pi e^2}{L^2\epsilon_0 q}\,\frac{1}{\pi}\,q\frac{L_z}{\pi}\,\frac{1}{\left(q\frac{L_z}{\pi}\right)^2+(n_2^{\lambda_2}-n_3^{\lambda_3})^2}[\,\delta_{n_1^{\lambda_1}-n_4^{\lambda_4},n_2^{\lambda_2}-n_3^{\lambda_3}}(1+\delta_{n_1^{\lambda_1}-n_4^{\lambda_4},0}) \\
& +\delta_{n_1^{\lambda_1}+n_4^{\lambda_4},n_2^{\lambda_2}-n_3^{\lambda_3}}]+\frac{2\pi e^2}{L^2\epsilon_0\, q}\,\frac{1}{\pi}\,q\frac{L_z}{\pi}\,\frac{1}{\left(q\frac{L_z}{\pi}\right)^2+(n_2^{\lambda_2}+n_3^{\lambda_3})^2}(\,\delta_{n_1^{\lambda_1}-n_4^{\lambda_4},n_2^{\lambda_2}+n_3^{\lambda_3}}+\delta_{n_1^{\lambda_1}+n_4^{\lambda_4},n_2^{\lambda_2}+n_3^{\lambda_3}}), \qquad \text{(A1)}
\end{aligned}
$$

$$
\begin{aligned}
V_{\vec{q}}^{m_1^{\lambda_1},n_2^{\lambda_2},n_3^{\lambda_3},m_4^{\lambda_4}} = {} & V_{\vec{q}}^{n_2^{\lambda_2},m_1^{\lambda_1},m_4^{\lambda_4},n_3^{\lambda_3}} \\
= {} & \frac{2\pi e^2}{L^2\epsilon_0 q}\,\frac{2}{\pi^2}\left(q\frac{L_z}{\pi}\right)^2(e^{-qL_z}-1)\left[\frac{\cos\left((n_2^{\lambda_2}-n_3^{\lambda_3})\frac{\pi}{2}\right)}{\left(q\frac{L_z}{\pi}\right)^2+(n_2^{\lambda_2}-n_3^{\lambda_3})^2}+\frac{\cos\left((n_2^{\lambda_2}+n_3^{\lambda_3})\frac{\pi}{2}\right)}{\left(q\frac{L_z}{\pi}\right)^2+(n_2^{\lambda_2}+n_3^{\lambda_3})^2}\right] \\
& \times\left[\frac{\cos\left((m_1^{\lambda_1}-m_4^{\lambda_4})\frac{\pi}{2}\right)}{\left(q\frac{L_z}{\pi}\right)^2+(m_1^{\lambda_1}-m_4^{\lambda_4})^2}-\frac{\cos\left((m_1^{\lambda_1}+m_4^{\lambda_4})\frac{\pi}{2}\right)}{\left(q\frac{L_z}{\pi}\right)^2+(m_1^{\lambda_1}+m_4^{\lambda_4})^2}\right]+\frac{2\pi e^2}{L^2\epsilon_0 q}\,\frac{1}{\pi}q\frac{L_z}{\pi}\,\frac{1}{\left(q\frac{L_z}{\pi}\right)^2+(n_2^{\lambda_2}-n_3^{\lambda_3})^2} \\
& \times[\,\delta_{m_1^{\lambda_1}-m_4^{\lambda_4},n_2^{\lambda_2}-n_3^{\lambda_3}}(1+\delta_{m_1^{\lambda_1}-m_4^{\lambda_4},0})-\delta_{m_1^{\lambda_1}+m_4^{\lambda_4},n_2^{\lambda_2}-n_3^{\lambda_3}}]+\frac{2\pi e^2}{L^2\epsilon_0 q}\,\frac{1}{\pi}q\frac{L_z}{\pi}\,\frac{1}{\left(q\frac{L_z}{\pi}\right)^2+(n_2^{\lambda_2}+n_3^{\lambda_3})^2} \\
& \times(\,\delta_{m_1^{\lambda_1}-m_4^{\lambda_4},n_2^{\lambda_2}+n_3^{\lambda_3}}-\delta_{m_1^{\lambda_1}+m_4^{\lambda_4},n_2^{\lambda_2}+n_3^{\lambda_3}}), \qquad \text{(A2)}
\end{aligned}
$$

$$V_{\vec{q}}^{m_1^{\lambda_1},m_2^{\lambda_2},m_3^{\lambda_3},m_4^{\lambda_4}}=\frac{2\pi e^2}{L^2\epsilon_0 q}\frac{2}{\pi^2}\left(q\frac{L_z}{\pi}\right)^2(e^{-qL_z}-1)\left[\frac{\cos\left((m_2^{\lambda_2}-m_3^{\lambda_3})\frac{\pi}{2}\right)}{\left(q\frac{L_z}{\pi}\right)^2+(m_2^{\lambda_2}-m_3^{\lambda_3})^2}-\frac{\cos\left((m_2^{\lambda_2}+m_3^{\lambda_3})\frac{\pi}{2}\right)}{\left(q\frac{L_z}{\pi}\right)^2+(m_2^{\lambda_2}+m_3^{\lambda_3})^2}\right]$$

$$\times\left[\frac{\cos\left((m_1^{\lambda_1}-m_4^{\lambda_4})\frac{\pi}{2}\right)}{\left(q\frac{L_z}{\pi}\right)^2+(m_1^{\lambda_1}-m_4^{\lambda_4})^2}-\frac{\cos\left((m_1^{\lambda_1}+m_4^{\lambda_4})\frac{\pi}{2}\right)}{\left(q\frac{L_z}{\pi}\right)^2+(m_1^{\lambda_1}+m_4^{\lambda_4})^2}\right]+\frac{2\pi e^2}{L^2\epsilon_0 q}\frac{1}{\pi}q\frac{L_z}{\pi}\frac{1}{\left(q\frac{L_z}{\pi}\right)^2+(m_2^{\lambda_2}-m_3^{\lambda_3})^2}$$

$$\times(\delta_{m_1^{\lambda_1}-m_4^{\lambda_4},m_2^{\lambda_2}-m_3^{\lambda_3}}(1+\delta_{m_1^{\lambda_1}-m_4^{\lambda_4},0})-\delta_{m_1^{\lambda_1}+m_4^{\lambda_4},m_2^{\lambda_2}-m_3^{\lambda_3}})+\frac{2\pi e^2}{L^2\epsilon_0 q}\frac{1}{\pi}q\frac{L_z}{\pi}\frac{1}{\left(q\frac{L_z}{\pi}\right)^2+(m_2^{\lambda_2}+m_3^{\lambda_3})^2}$$

$$\times(-\delta_{m_1^{\lambda_1}-m_4^{\lambda_4},m_2^{\lambda_2}+m_3^{\lambda_3}}+\delta_{m_1^{\lambda_1}+m_4^{\lambda_4},m_2^{\lambda_2}+m_3^{\lambda_3}}),\tag{A3}$$

$$V_{\vec{q}}^{m_1^{\lambda_1},m_2^{\lambda_2},n_3^{\lambda_3},n_4^{\lambda_4}}=V_{\vec{q}}^{n_4^{\lambda_4},n_3^{\lambda_3},m_2^{\lambda_2},m_1^{\lambda_1}}$$

$$=\frac{2\pi e^2}{L^2\epsilon_0 q}\frac{2}{\pi^2}\left(q\frac{L_z}{\pi}\right)^2(e^{-qL_z}+1)\left[\frac{\sin\left((m_2^{\lambda_2}-n_3^{\lambda_3})\frac{\pi}{2}\right)}{\left(q\frac{L_z}{\pi}\right)^2+(m_2^{\lambda_2}-n_3^{\lambda_3})^2}+\frac{\sin\left((m_2^{\lambda_2}+n_3^{\lambda_3})\frac{\pi}{2}\right)}{\left(q\frac{L_z}{\pi}\right)^2+(m_2^{\lambda_2}+n_3^{\lambda_3})^2}\right]$$

$$\times\left[-\frac{\sin\left((m_1^{\lambda_1}-n_4^{\lambda_4})\frac{\pi}{2}\right)}{\left(q\frac{L_z}{\pi}\right)^2+(m_1^{\lambda_1}-n_4^{\lambda_4})^2}-\frac{\cos\left((m_1^{\lambda_1}+n_4^{\lambda_4})\frac{\pi}{2}\right)}{\left(q\frac{L_z}{\pi}\right)^2+(m_1^{\lambda_1}+n_4^{\lambda_4})^2}\right]+\frac{2\pi e^2}{L^2\epsilon_0 q}\frac{1}{\pi}q\frac{L_z}{\pi}\frac{1}{\left(q\frac{L_z}{\pi}\right)^2+(m_2^{\lambda_2}-n_3^{\lambda_3})^2}$$

$$\times(\delta_{m_1^{\lambda_1}-n_4^{\lambda_4},m_2^{\lambda_2}-n_3^{\lambda_3}}+\delta_{m_1^{\lambda_1}+n_4^{\lambda_4},m_2^{\lambda_2}-n_3^{\lambda_3}})+\frac{2\pi e^2}{L^2\epsilon_0 q}\frac{1}{\pi}q\frac{L_z}{\pi}\frac{1}{\left(q\frac{L_z}{\pi}\right)^2+(m_2^{\lambda_2}+n_3^{\lambda_3})^2}$$

$$\times(\delta_{m_1^{\lambda_1}-n_4^{\lambda_4},m_2^{\lambda_2}+n_3^{\lambda_3}}+\delta_{m_1^{\lambda_1}+n_4^{\lambda_4},m_2^{\lambda_2}+n_3^{\lambda_3}}),\tag{A4}$$

$$V_{\vec{q}}^{n_1^{\lambda_1},n_2^{\lambda_2},n_3^{\lambda_3},m_4^{\lambda_4}}=0,\tag{A5}$$

$$V_{\vec{q}}^{n_1^{\lambda_1},n_2^{\lambda_2},m_3^{\lambda_3},n_4^{\lambda_4}}=0,\tag{A6}$$

$$V_{\vec{q}}^{n_1^{\lambda_1},m_2^{\lambda_2},n_3^{\lambda_3},n_4^{\lambda_4}}=0,\tag{A7}$$

$$V_{\vec{q}}^{m_1^{\lambda_1},n_2^{\lambda_2},n_3^{\lambda_3},n_4^{\lambda_4}}=0,\tag{A8}$$

$$V_{\vec{q}}^{m_1^{\lambda_1},m_2^{\lambda_2},m_3^{\lambda_3},n_4^{\lambda_4}}=0,\tag{A9}$$

$$V_{\vec{q}}^{m_1^{\lambda_1},m_2^{\lambda_2},n_3^{\lambda_3},m_4^{\lambda_4}}=0,\tag{A10}$$

$$V_{\vec{q}}^{m_1^{\lambda_1},n_2^{\lambda_2},m_3^{\lambda_3},m_4^{\lambda_4}}=0,\tag{A11}$$

$$V_{\vec{q}}^{n_1^{\lambda_1},m_2^{\lambda_2},m_3^{\lambda_3},m_4^{\lambda_4}}=0.\tag{A12}$$

This concludes the presentation of the different Coulomb potential terms.

APPENDIX B: THE WAVE-PROPAGTION SOLUTION

In this appendix we have written down the wave-propagation solution. Here, $n_x^{\lambda_x}$ labels the quantized states $n_x^{\lambda_x} = 1, 3, 5, 7, \ldots$ and $m_x^{\lambda_x}$ labels the quantized states $m_x^{\lambda_x} = 2, 4, 6, 8, \ldots$,

$$E_T^{n_1^v,n_2^c}(z,\omega)=\frac{4\pi}{L_z}\frac{c^2}{c_0^2}d_{cv}P_{n_1^v,n_2^c}(\omega)\left(\frac{\cos\left((n_1^v-n_2^c)\frac{\pi}{L_z}z\right)}{(n_1^v-n_2^c)^2\frac{\pi^2c^2}{L_z^2\omega^2}-1}+\frac{\cos\left((n_1^v+n_2^c)\frac{\pi}{L_z}z\right)}{(n_1^v+n_2^c)^2\frac{\pi^2c^2}{L_z^2\omega^2}-1}\right)$$
$$+t_{n_1^v,n_2^c}(\omega)e^{i(\omega/c)z}+r_{n_1^v,n_2^c}(\omega)e^{-i(\omega/c)z}, \tag{B1}$$

$$E_T^{m_1^v,m_2^c}(z,\omega)=\frac{4\pi}{L_z}\frac{c^2}{c_0^2}d_{cv}P_{m_1^v,m_2^c}(\omega)\left(\frac{\cos\left((m_1^v-m_2^c)\frac{\pi}{L_z}z\right)}{(m_1^v-m_2^c)^2\frac{\pi^2c^2}{L_z^2\omega^2}-1}-\frac{\cos\left((m_1^v+m_2^c)\frac{\pi}{L_z}z\right)}{(m_1^v+m_2^c)^2\frac{\pi^2c^2}{L_z^2\omega^2}-1}\right)$$
$$+t_{m_1^v,m_2^c}(\omega)e^{i(\omega/c)z}+r_{m_1^v,m_2^c}(\omega)e^{-i(\omega/c)z}, \tag{B2}$$

$$E_T^{m_1^v,n_2^c}(z,\omega)=\frac{4\pi}{L_z}\frac{c^2}{c_0^2}d_{cv}P_{m_1^v,n_2^c}(\omega)\left(\frac{\sin\left((m_1^v-n_2^c)\frac{\pi}{L_z}z\right)}{(m_1^v-n_2^c)^2\frac{\pi^2c^2}{L_z^2\omega^2}-1}+\frac{\sin\left((m_1^v+n_2^c)\frac{\pi}{L_z}z\right)}{(m_1^v+n_2^c)^2\frac{\pi^2c^2}{L_z^2\omega^2}-1}\right)$$
$$+t_{m_1^v,n_2^c}(\omega)e^{i(\omega/c)z}+r_{m_1^v,n_2^c}(\omega)e^{-i(\omega/c)z}, \tag{B3}$$

$$E_T^{n_1^v,m_2^c}(z,\omega)=\frac{4\pi}{L_z}\frac{c^2}{c_0^2}d_{cv}P_{n_1^v,m_2^c}(\omega)\left(\frac{\sin\left((m_2^c-n_1^v)\frac{\pi}{L_z}z\right)}{(n_1^v-m_2^c)^2\frac{\pi^2c^2}{L_z^2\omega^2}-1}+\frac{\sin\left((n_1^v+m_2^c)\frac{\pi}{L_z}z\right)}{(n_1^v+m_2^c)^2\frac{\pi^2c^2}{L_z^2\omega^2}-1}\right)$$
$$+t_{n_1^v,m_2^c}(\omega)e^{i(\omega/c)z}+r_{n_1^v,m_2^c}(\omega)e^{-i(\omega/c)z}, \tag{B4}$$

[1] See, for a textbook discussion, H. Haug and S. W. Koch, *Quantum Theory of the Optical and Electronic Properties of Semiconductors* (World Scientific, Singapore, 1993).

[2] See, for a textbook discussion, A. Stahl and I. Balslev, *Electrodynamics of the Semiconductor Band Edge*, Springer Tracts in Modern Physics Vol. 110 (Springer-Verlag, Berlin, 1987).

[3] T. Stroucken, A. Knorr, P. Thomas, and S. W. Koch, Phys. Rev. B **53**, 2026 (1996).

[4] L. C. Andreani and A. Pasquarello, Phys. Rev. B **42**, 8928 (1990).

[5] R. Zimmermann, Adv. Solid State Phys. **30**, 295 (1990).

[6] X.-F. He, Phys. Rev. B **43**, 2063 (1991).

[7] R. Zimmermann, *Excitonic Spectra in Semiconductor Nanostructures*, Proceedings of the International Conference on Optical Properties of Nanostructures [Jpn. J. Appl. Phys. Suppl. **34**, 228 (1995)].